Heliyon 11 (2025) e42317

Contents lists available at ScienceDirect

Heliyon

journal homepage: www.cell.com/heliyon

Research article

Electrochemical Corrosion Performance of N80 steel in Acidized 10% HCl medium using 4-methyl-1-Phenyl-3-(*p*-tolyldiazenyl) −2,3-dihydro-1H-pyrrol-2-ol

Reham H. Wahba [a], Adel Z. El-Sonbati [a], Mostafa A. Diab [a], Esam A. Gomaa [b], Marwa N. El-Nahass [c], Y.M. Abdallah [d,*]

[a] *Chemistry Department, Faculty of Science, Damietta University, Egypt*
[b] *Chemistry Department, Faculty of Science, Mansoura University, Mansoura, Egypt*
[c] *Department of Chemistry, Faculty of Science, Tanta University, Tanta, 31527, Egypt*
[d] *Delta University for Science and Technology, Gamasa, Mansoura, 11152, Egypt*

ARTICLE INFO

Keywords:
MPTHP azo-dye
Acidized 10% HCl medium
Corrosion inhibition
DFT
Monte Carlo (MC)
EIS

ABSTRACT

Background: In this study, the azo dye, 4-methyl-1-phenyl-3-(p-tolyldiazenyl)-2,3-dihydro-1H-pyrrol-2-ol **(MPTHP)** was synthesized and estimated as a novel inhibitor for protecting N80 steel from corrosion in a 10 % HCl acidic environment.
Methods: Potentiodynamic polarization (PP) and electrochemical impedance spectroscopy (EIS) methods were employed. Additionally, Monte Carlo (MC) simulations and density functional theory (DFT) were utilized to establish a link between the protective capacity and the molecular structure of the inhibitor.
Significant findings: The inhibitor confirmed an impressive inhibition prohibition of 91 % when its concentration was increased to 1×10^{-4} M at 25 ± 1 °C, as determined by EIS analysis. PP analysis indicated that the MPTHP azo-dye compound functions as a mixed-type inhibitor and chemisorbs onto the surface of N80 steel. Furthermore, the Langmuir adsorption isotherm was found to be the most suitable model to describe the adsorption of the examined compound. This research has the potential to introduce MPTHP as an innovative corrosion inhibitor for preventing N80 steel corrosion in various industrial settings, particularly in pickling solutions.

1. Introduction

Issues with the environment and the economy caused by metal corrosion are significant. According to estimates, the recorded loss will affect the gross national product (GNP) of several nations by 1–5 % [1]. It is understood that corrosion is an unfavorable electrochemical procedure that ensues between the metal and its surroundings. The rate of material deterioration increases with the duration of exposure to the environment. As a result, the development of protective methods has been vigorously pursued and is now crucial to lowering the cost of corrosion [2–5]. One method is the use of organic components to prevent corrosion, which has led to significant growth in attention across several industries [6–8]. This protective method's effectiveness, viability, affordability, and minimal toxicity are all cited as reasons for its success [9–11].

* Corresponding author.
E-mail addresses: Yasser.Mostafa@deltauniv.edu.eg, dr.ymostafa8@gmail.com (Y.M. Abdallah).

https://doi.org/10.1016/j.heliyon.2025.e42317
Received 23 December 2024; Accepted 27 January 2025
Available online 30 January 2025

Applications for carbon steel in engineering and industry, such as design and construction, are numerous. Unfortunately, the main drawback of employing carbon steel is that it is easily corroded [12]. A typical method of industrial cleaning used in the creation of lubricants and petrochemicals is acid pickling. Its primary purpose is to eliminate mineral oxides and deposits of mineral scale. However, it is crucial to remember that the use of mineral acid, such as HCl, in this process can lead to significant corrosion-related concerns due to its highly corrosive nature [13].

Environmentally, friendly organic inhibitors have been developed to meet increasing demands. Generally, organic substances that include oxygen, sulfur, nitrogen, aromatic rings, and heterocyclic structures are adsorbed onto metal surfaces and exhibit effective inhibition due to their interaction with the metal's *d*-orbitals [14]. The selection of suitable inhibitors depends on factors such as acid type and concentration, temperature, organic or inorganic materials that have dissolved, as well as the kind of metal that is being shielded [15]. Azo dyes, a significant group of organic substances that are frequently utilized in leather, cosmetics, textiles, pharmaceuticals, and as corrosion inhibitors, are notable among these compounds [16,17]. For instance, they serve as carbon steel corrosion inhibitors [18–20], mild steel [21,22], and aluminum [23,24], involving the azo group and substituted aromatic bonds on the metal surface engaging in chemical reactions. Through this process, the molecule acquires unique color throughout the visible light spectrum. while also enhancing metal stability, reducing production costs, and employing straightforward synthetic methods [25,26].

This paper's objective is to evaluate the performance 4-Methyl-1-Phenyl-3-(p-Tolyldiazenyl)-2,3-Dihydro-1H-Pyrrol-2-ol **(MPTHP)** as an effective and environmentally friendly corrosion inhibitor for N80 steel in an acidic solution (10% HCl) using electrochemical techniques like potentiodynamic polarization (PP) and electrochemical impedance spectroscopy (EIS). The organic compound's abundance of π-electrons and heteroatoms, such as nitrogen and oxygen atoms, result in increased adsorption on the steel surface as compared to other organic inhibitors, which is why this dye was chosen. To achieve this, we first established an adsorption isotherm model at 298 K, allowing us to compute key parameters, including K_{ads} (adsorption equilibrium constant) and ΔG^{o}_{ads} (standard Gibbs free energy change for adsorption), consistent with the Langmuir isotherm model. This revealed that the adsorption process follows a chemisorption mechanism. To gain deeper insights into the active centers and corrosion prevention mechanisms associated with the tested **MPTHP** compound, we employed quantum chemical computations (DFT) and molecular dynamics (MD) simulations. This comprehensive analysis included the determination of Fukui indices, Mulliken atomic charges, and the mapping of electrostatic potential (MEP). These advanced computational techniques provided valuable information about the compound's behavior and its ability to mitigate corrosion reactions on N80 steel, enhancing our understanding of its protective capabilities. Also, we can illustrate the inhibition mechanism as the adsorption process may start with -Cl^- anions being initially adsorbed on protonated steel surfaces to generate a negatively charged barrier because it is well recognized that N80 steel surfaces are (+ve) charged in hydrochloric acid solutions.

2. Materials and techniques

2.1. Materials and solutions

Chemical components were procured from commercial suppliers and used without further purification. *p*-methyl aniline, 4-methyl-1-phenyl-1H-pyrrol-2(3H)-one and sodium nitrite were obtained from Sigma-Aldrich Chemical Co. (St. Louis, MO, USA). N80 carbon steel electrode [composition (weight %): C (0.31 %), S (0.008 %), P (0.01 %), Si (0.19 %), Mn (0.92 %), Cr (0.20 %), and the rest Fe] of rectangular shape with a real exterior area of about 1 cm^2 was employed as the active electrode in this study. The electrode was grazed with several grades of emery papers (up to 1200 grade), degreased with acetone, cleaned with bi-distilled water, and dried with paper. The experiments were carried out in acidized 10 % hydrochloric acid solutions, with and without many dosages of the examined MPTHP azo dye, as reported in Table 1. The concentrations of the tested inhibitor ranged from 1×10^{-6} M to 1×10^{-4} M for each experiment, and a freshly prepared solution was used each time.

2.1.1. Synthesis of 4-methyl-1-Phenyl-3-(p-Tolyldiazenyl)-2,3-Dihydro-1H-Pyrrol-2-ol (MPTHP)

In a standard preparation, 0.01 mol of hydrochloric acid was added to 25 ml of distilled water containing *p*-methyl aniline. After

Table 1
The studied inhibitor's chemical formula, molecular weight, and structure.

Compound	Name	Structure	Molecular Weight& Chemical Formula
MPTHP	**4-methyl-1-phenyl-3-(p-tolyldiazenyl)-2,3-dihydro-1H-pyrrol-2-ol**	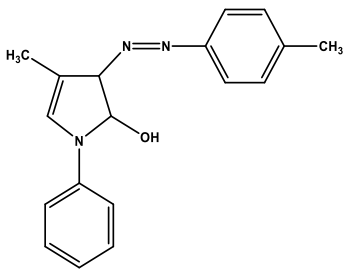	**$C_{18}H_{19}N_3O$ 293.37**

stirring and cooling the mixture to 0 °C, a solution of 0.01 mol sodium nitrite in 20 ml of water was added dropwise to the resultant liquid. As seen in Scheme 1, the produced diazonium chloride was next combined with an alkaline solution of 0.01 mol 4-methyl-1-phenyl-1H-pyrrol-2(3H)-one. The instantly generated colored precipitate was filtered through a glass crucible that had been sintered and repeatedly cleaned with water. The purity of the prepared **MPTHP** was examined using elemental examination, IR, and ^{1}H NMR spectra: Microanalysis. Found (%), C, 74.80; H, 5,60, N, 14.40. Calcd for $C_{18}H_{19}N_3O$ (%): C 74.20. H. 5.88; N, 14.42 IR (KBr, υ_{max}, cm): 3430 (N-H. str.), 1595 (C=N- str.). H NMR (6, ppm): 11.20 (NH, hydrazone, exchangeable with D_2O).

2.2. Electrochemical techniques

In each experiment, trials were conducted at a stable temperature of 25±1 °C, following a 30-min stabilization period for the electrode potential. To ensure consistency and reliability, all tests were systematically performed under identical conditions. We employed three derivative electrodes in conjunction with the CS Potentiostat/Galvanostat electrochemical workstation CS350. All potential measurements were referenced to an Ag/AgCl electrode. The counter electrode used was a platinum electrode with a surface area of 1 cm^2.

After 30 min of submerging the working electrode in the corrosive media and reaching a steady state, we measured the open circuit potential (OCP). Tafel polarization graphs were produced by varying electrode potentials between −0.6 V and 0.2 V relative to the OCP. This process was conducted in an air-saturated environment under potentiodynamic conditions; with a sweep rate of 1 mV/s. Multiple electrode potentials in the same range of −0.6 –0.2 V were combined to construct the Tafel polarization curves with respect to the OCP. All experiments were conducted using an N80 carbon steel electrode in acidified 10 % HCl at 25 °C, both with and without varying portions of the studied inhibitor.

To calculate cathodic and anodic Tafel data for charge transfer-measured corrosion responses, we determined the values of (log i_{corr}) and the equivalent corrosion potential (E_{corr}) in the acidified 10 % HCl solution, considering all concentrations of the investigated inhibitor (**MPTHP**). This was accomplished using the Stern-Geary process [27,28] was accepted. Surface coverage (θ) and inhibitory proficiency (η) were designed via **equation (1)**:

$$\%\eta = \theta \times 100 = \left(1 - \frac{i_{corr\ (inh)}}{i_{corr\ (free)}}\right) \times 100 \quad (1)$$

where, respectively, $i_{corr\ (free)}$ and $i_{corr\ (inh)}$ represent corrosion current densities with and without doses of the examined **MPTHP**.

Electrochemical impedance spectroscopy (EIS) dimensions were achieved on the same cell that was utilized for potentiodynamic polarization (PP) studies. The EIS was achieved consuming ac signals at OCP with a signal amplitude agitation of 10 mV peak-to-peak spanning the frequency variety of 100 mHz to 100 kHz. The considered compliant circuit was used to measure and clarify impedance testing results.

The polarization resistance R_p and the double layer capacity C_{dl} are the suggested variables resulting from the study of Nyquist semicircles.

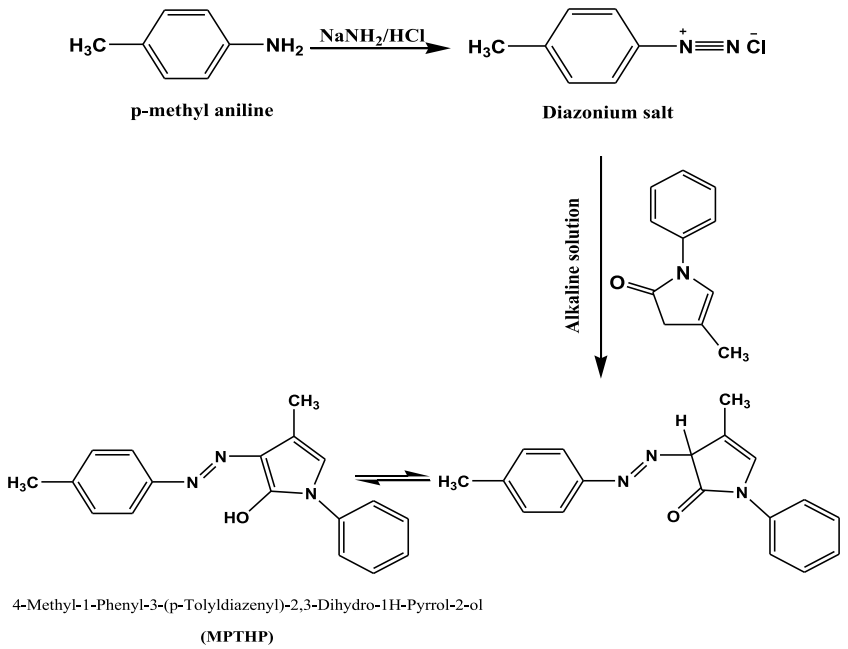

Scheme 1. Synthesis of 4-Methyl-1-Phenyl-3-(*p*-Tolyldiazenyl)-2,3-Dihydro-1H-Pyrrol-2-ol (MPTHP).

$$C_{dl} = \left(Y_o\, R_{ct}^{1-n}\right)^{1/n} \quad (2)$$

Y_o is the CPE constant, and n is the CPE exponent in this equation. The divergence from optimal behavior is indicated by the value of n, which ranges from 0 to 1 [29].

The following equation is used to construct the impedance technique's surface coverage (θ) and inhibitory capacity (%η):

$$\%\,\eta = \theta \times 100 = \left(1 - \left[\frac{R_{ct}^{\circ}}{R_{ct}}\right]\right) \times 100 \quad (3)$$

where R_{ct}^{o} and R_{ct} stand for the charge transfer resistance values with and without **MPTHP**, respectively.

2.3. Quantum chemical calculations (DFT) and MC simulations

The relationship between theoretically calculations and investigational results to detected inhibition efficiencies have been assessed efficiently for stable corrosion [30]. Theoretical investigations were conducted using Accelrys Materials Studio 7.0, employing the $DMol^3$ module for Density Functional Theory (DFT) designs and the adsorption locator module for Monte Carlo (MC) simulations. In the DFT calculations, the constructions of the inhibitor molecules under examination were optimized. This optimization process utilized the GGA/BLYP functional and the DNP 4.4 basis set and a convergence criterion on the forces on atoms smaller than 0.005 eV/Å. Additionally, COSMO solvation controls were applied to account for solvation effects, ensuring a more accurate representation of the molecular structures and properties [30]. The most effective **MPTHP** particle adsorption configurations on the Fe (1 1 0) exterior were found using the adsorption locator module in the Monte Carlo (MC) simulations. This included systematically examining **MPTHP** particle arrangements using Monte Carlo methods, which then allowed for an evaluation of their protective effectiveness on the Fe (1 1 0) exterior [31]. With the assigned COMPASS force field, **MPTHP** particle, water molecule, and Fe (1 1 0) surface adsorption was completed in a simulated container (32.27 × 32.27 × 50.18 $Å^3$) [32]. Additionally, in our prior work that was published, we incorporated all of the inputs, outputs, and computations from computational investigations [30,31].

3. Results and discussion

3.1. Potentiodynamic polarization (PP) calculations

3.1.1. Effect of the MPTHP component concentrations

Using the potentiodynamic polarization technique (PP) at 25 °C, the corrosion presentation of N80 steel in an acidified 10 % HCl medium was examined. Cathodic-anodic plots were completed both while present and when not of various doses of **MPTHP**. As revealed in Fig. 1, for the investigated component, a satisfactory study for the polarization plots with cathodic and anodic Tafel shapes were showed, and kinetic variables were designed in Table 2, as corrosion potential (**E_{corr}**), corrosion current density (**I_{corr}**) consequential from polarization plots by extrapolation, anodic (**β_a**) and cathodic (**β_c**) Tafel slopes, the surface coverage (**θ**), in accumulation to the inhibition productivity (%η) which attained by **Eq. (1)**.

Lines of Tafel polarization diagrams, anodic and cathodic plots were evacuated in the attendance of the thought-of inhibitor, resulting in low current densities with increasing the **MPTHP** concentrations [33], which suggesting that **MPTHP** inhibitor is mixed-type. The corrosion current density diminishes from 88.44 μA.cm^{-2} (Blank) to 8.3 μA.cm^{-2} in case of 1 × 10^{-4} M concentration.

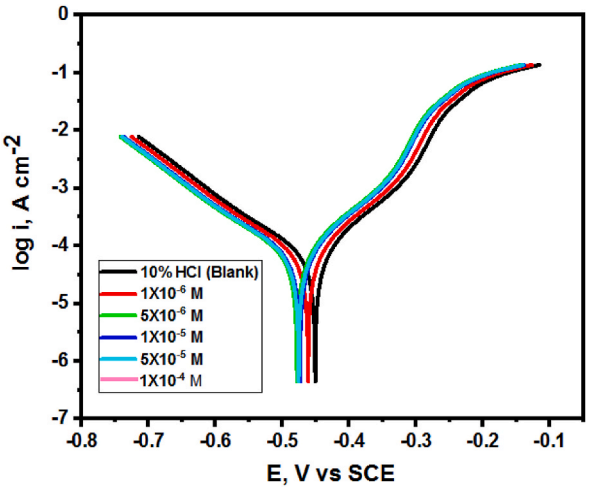

Fig. 1. Anodic and cathodic Tafel polarization curves for the corrosion of N80 steel in acidized 10 % HCl solution in the presence and absence of various **MPTHP** concentrations at 25 ± 1 °C.

Table 2
The electrochemical parameters computed for the corrosion of N80 carbon steel in acidized 10 % HCl solution in the absence and presence of various concentrations of the tested **MPTHP** at 25 ± 1 °C using the potentiodynamic polarization technique.

Conc. M,	- E_{corr}, mV	i_{corr}, μAcm^{-2}	βa, $mVdec^{-1}$	βc, $mVdec^{-1}$	C.R. mmy^{-1}	θ	η %
0.00 (Blank)	428.42	88.44	69.713	103.55	1.0375	0.00	0.00
1×10^{-6}	459.34	58.5	86.543	107.321	0.984	0.339	33.9
5×10^{-6}	451.13	41.6	102.53	142.52	0.8317	0.529	52.9
1×10^{-5}	455.38	22.65	80.876	115.94	0.6058	0.744	74.4
5×10^{-5}	452.95	11.5	86.073	128.75	0.8036	0.870	87.0
1×10^{-4}	458.45	8.3	87.597	118.78	0.4139	0.906	90.6

By cumulative the MPTHP concentration from 1×10^{-6} M to 1×10^{-4} M, the inhibition proficiency (%η) increased as demonstrated in Table 2. A small improvement in the corrosion potential **(E_{corr})** is made by adding of **MPTHP** component, the anodic and cathodic Tafel slopes (**β_a** & **β_c**) values altered with cumulative concentrations, indicating that the **MPTHP** compound was deceptive in mechanism of dissolution and hydrogen evolution processes, confirming the studied inhibitor's mixed-type nature [34,35].

3.1.2. Adsorption isotherm

The **MPTHP** component under investigation confers a delay in the corrosion process on the compound's adsorption mechanism on a sample of N80 carbon steel. Equation (4) describes the **MPTHP** compound adsorption at the metal/solution surface, which happens when **MPTHP** particles replace water particles [36].

$$\text{MPTHP}_{(sol)} + x\text{H}_2\text{O}_{(ads)} \rightarrow \text{MPTHP}_{(ads)} + x\text{H}_2\text{O}_{(sol)} \quad (4)$$

The **MPTHP** compounds in solution and adsorbed on the surface of N80 carbon steel, consistently, are designated as $\text{MPTHP}_{(sol)}$ and $\text{MPTHP}_{(ads)}$. x represents how many water particles were swapped out for **MPTHP** particles.

To calculate the surface coverage (θ) by **MPTHP** components, use the following equation;

$$\theta = \left[1 - \frac{i_{corr}}{i^{o}_{corr}}\right] \quad (5)$$

In our study, the parameter θ was subjected to various adsorption isotherm models to determine the most appropriate model that fits the experimental data. The analysis revealed that the MPTHP inhibitor under investigation displayed a virtuous fitting to the Langmuir isotherm model. This finding is summarized in Equation (6), which simplifies the connection between C (concentration) and C/θ, resulting in a linear association with a coefficient constant (R^2) nearly unity at a temperature of 25±1 °C and a slope equal to unity, as illustrated in (Fig. 2).

$$\frac{C}{\theta} = \frac{1}{K_{ads}} + C \quad (6)$$

where "C are the **MPTHP** concentrations and $\mathbf{K_{ads}}$ is the equilibrium constant for adsorption method" that is associated to the common adsorption free energy (ΔG°_{ads}) and may be taken into consideration using Equation (7) [37].

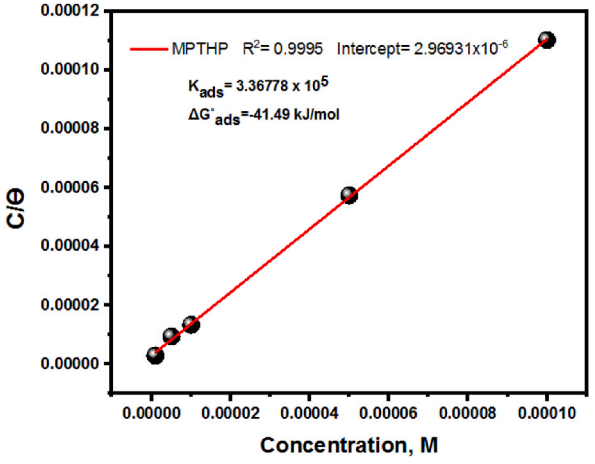

Fig. 2. Langmuir isotherm plot for N80 steel corrosion in acidized 10 % HCl solution in the existence of various dosages of **MPTHP** at 25 ± 1 °C.

$$K_{ads} = \frac{1}{55.5}\exp\left(\frac{-\Delta G^{\circ}_{ads}}{RT}\right) \quad (7)$$

The parameter θ, derived from the potentiodynamic polarization (PP) performance, was employed to evaluate various adsorption isotherm models. This analysis aimed to recognize the most appropriate adsorption isotherm, and it was confirmed that the adsorption of MPTHP on the N80 surface, as depicted in (Fig. 2), adhered well to the Langmuir adsorption isotherm.

The equation used to describe this behavior takes into account the water concentration (55.5 mol/L), the absolute temperature (T) in Kelvin, and the universal gas constant (R), as key factors influencing the adsorption process [38,39].

The standard free energy of adsorption (ΔG°_{ads}), designed by Equation (7), is designed in Table 3. The greater values of ($\mathbf{\Delta G^{\circ}_{ads}}$) (i.e., −40 kJ mol^{-1} or more) and the (-ve) sign of ($\mathbf{\Delta G^{\circ}_{ads}}$) values comprise charge transfer with the examined MPTHP compound compared to the steel exterior to process a coordinate bond (chemisorption adsorption) [40] and allow for the examined **MPTHP** compound to spontaneously adhere on the steel metal [41]. Additionally, the **MPTHP** component's $\mathbf{\Delta G^{\circ}_{ads}}$ value is nearly steady for steel surfaces thanks to coordination bonds that form between the active centers of the validated **MPTHP** (*N*-atoms, *P*-orbitals of double bonds), and the unoccupied *d*-orbitals of the steel metal.

3.2. Electrochemical impedance spectroscopy (EIS designs)

Figs. 3 and 4 display, respectively, the Nyquist and Bode designs for N80 steel in acidized 10% HCl solutions in both with and without different doses of **MPTHP** molecules. The radius of Nyquist semicircles is what determines the charge transfer resistance, or $\mathbf{R_{ct}}$, and going forward, $\mathbf{R_{ct}}$ values rise with rising concentrations (i.e., the semicircle radius rises).

For the uninhibited and inhibited solutions, a one-time constant was identified in Nyquist and Bode designs at small frequencies, demonstrating the creation of a protecting film on steel exterior [42,43].

The associated electrical circuit design, where $\mathbf{R_s}$ is the solution resistance, $\mathbf{R_{ct}}$ is **MPTHP** polarized resistance, and CPE is the constant phase element of the tested component, was projected to take into account the acquired impedance surveys and is intended in Fig. 5.

The polarization resistance $\mathbf{R_{ct}}$ attained from the EIS approach, the preventive proficiency for the corrosion of N80 steel (%η) in acidized 10 % HCl using the following formulae [44,45]:

$$\%\eta = \theta \times 100 = \left(1 - \left[\frac{R^{o}_{ct}}{R_{ct}}\right]\right) \quad (8)$$

where R°_{ct} and R_{ct} are the charge transfer resistance of N80 samples in acidized 10 % HCl solutions with and without the **MPTHP** compound, correspondingly.

According to Table 4, the heterogeneity of the steel samples is shown by the change in the exponent '*n*' values by 0.756 and 0.904, which shows that a number of components are those who work on the adsorption method on the N80 surface. The N80 surface's own irregularity, the diffusion of active sites, the dissolving of metal, the presence of impurities, and the adsorption of **MPTHP** on the N80 steel metal are some of these elements. The system's non-ideal capacitive behavior, which is impacted by these intricate interconnections and surface properties, is reflected in the fluctuation of the '*n*' values. Additionally, the Y_0 value fell when the inhibitor was used, suggesting that either the electrical double layer's thickness grew or the local dielectric constant decreased. This implies that the way the azo molecules work is by covering the metal surface with a protective coating.

The electrochemical characteristics from the Electrochemical Impedance Spectroscopy (EIS) investigations are shown in Table 4 in the 10 % HCl corrosive environment, N80 steel showed higher values of $\mathbf{R_{ct}}$ (charge transfer resistance), which indicates efficient corrosion inhibition. The corrosion process may be hampered because of the **MPTHP** particles adhering to the N80 steel surface. Additionally, it suggests that the **MPTHP** inhibitor has exchanged the adsorbed water particles on the exterior, thus enhancing the protection of the tested surface [46–48].

The substantial reduction in the access of the CPE variables is caused by the adsorption of **MPTHP** compound on the tested surface, which rises the width of the electrical double layer and inhibitor coating layer which permits the adsorption of **MPTHP** particles on the tested metal.

Effectively of inhibition (%η) based on electrochemical impedance extents agree exactly with those based on polarization results.

- *Inhibition efficiency comparison with other inhibitors*

It is possible to compare the inhibitory effectiveness of MPTHP with other inhibitors that have been reported to protect carbon steel by using azo dye corrosion inhibitors. Table 5 demonstrates the high inhibitory effectiveness of the majority of the azo dyes tested. In comparison, MPTHP demonstrates the greatest inhibitory efficiency among the azo dyes mentioned in Table 5 [49–55] (Khalefa et al.,

Table 3
K_{ads} and ΔG^{o}_{ads} Values based on Langmuir isotherm.

Compound	Temperature, K	K_{ads}, M^{-1}	$-\Delta G^{o}_{ads}$, $kJmol^{-1}$
I; (MPTHP)	298	2.62E+05	40.86

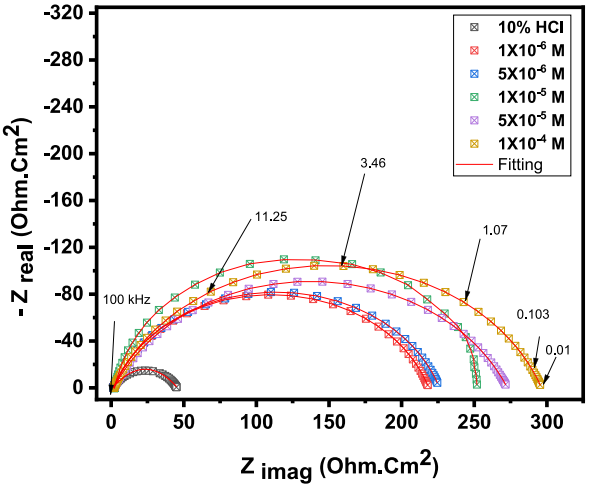

Fig. 3. Nyquist plots for the corrosion of N80 steel in acidized 10 % HCl solution with and without of various concentrations of the examined **MPTHP** at 25± 1 °C.

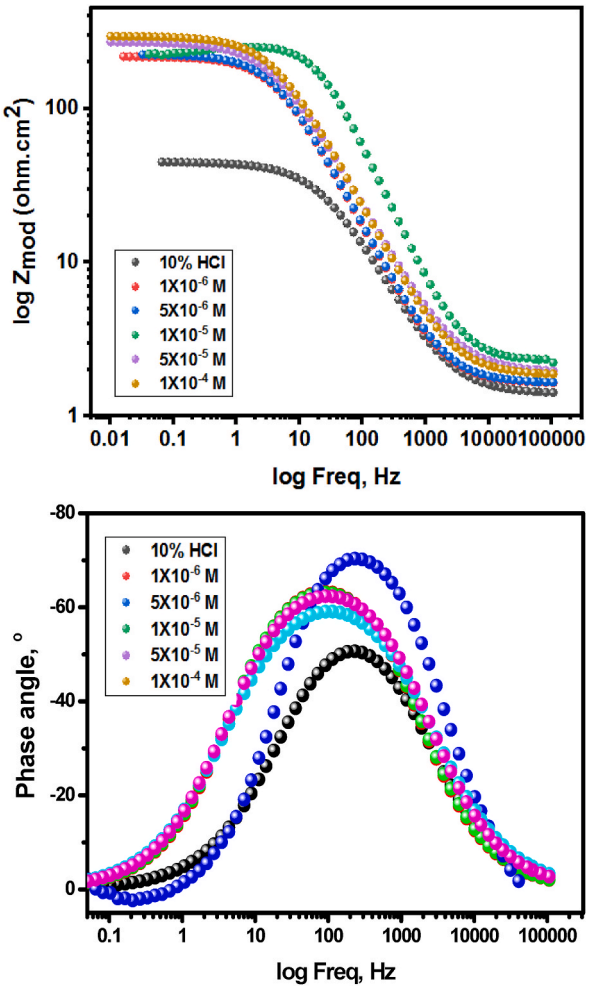

Fig. 4. Bode plots for the corrosion of N80 steel in acidized 10 % HCl solution with and without of various concentrations of the tested **MPTHP** at 25 ± 1 °C.

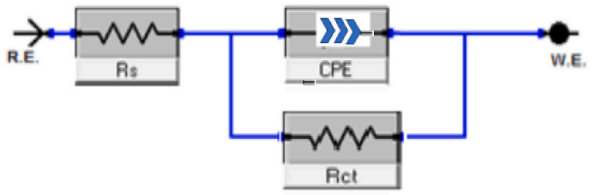

Fig. 5. The proper Electrical corresponding circuit used to fit EIS data.

Table 4
Electrochemical kinetic variables gained by the EIS method for the corrosion of N80 steel in 10 % HCl acidized solution with and without diverse concentrations of the tested **MPTHP** at 25 ± 1 °C.

Conc., M	R_s, Ω cm^2	R_{ct}, Ω cm^2	C_{dl} (μF cm^{-2})	CPE		θ	% IE
				$Y_0 \times 10^{-4}$, $\Omega^{-1}s\ cm^{-2}$	n		
0.00 (Blank)	1.3982 ± 0.0013	43.747	1.63×10^{-4}	5.431	0.75674 ± 0.007	0.00	0.00
1×10^{-6}	1.6342 ± 0.0016	217.01	1.73×10^{-4}	3.2717	0.80558 ± 0.008	0.798	79.8
5×10^{-6}	1.6487 ± 0.0016	224.42	1.72×10^{-4}	3.2717	0.80205 ± 0.008	0.805	80.5
1×10^{-5}	2.3712 ± 0.0023	255.23	3.99×10^{-4}	4.9616	0.90469 ± 0.009	0.829	82.9
5×10^{-5}	1.9234 ± 0.0019	369.44	1.68×10^{-4}	3.3471	0.75271 ± 0.007	0.882	88.2
1×10^{-4}	1.8535 ± 0.0018	485.56	1.58×10^{-4}	2.7375	0.78572 ± 0.007	0.91	91.0

2033; Amoko et al., 2018; Nagiub et al., 2013; Devika et al., 2020). Its efficiency is corresponding to that designated in Shalabi et al., 2024; Mabrouk et al., 2017; and Yusoff et al., 2020. It is evident that as the concentration of **MPTHP** increases, the rate of corrosion decreases and the inhibitive efficiency improves. This improvement is expected due to the increased adsorption coverage of the inhibitor on mild steel surfaces as the **MPTHP** concentration rises.

3.3. DFT calculations

DFT simulations were done to examine the contact between the steel exterior and the active centers of the **MPTHP** particles. HOMO and LUMO orbitals for the **MPTHP** derivative's optimized structures are exposed in Fig. 6, and Table 5 tilts the related quantum chemical variables. As stated by the FMO hypothesis, HOMO and LUMO energies determine whether an inhibitor component at the inhibitor/metal contact is a donor or an acceptor [56]. According to surveys, corrosion inhibitors with large E_{HOMO} and small E_{LUMO} values are supposed to be incredibly effective. According to Table 5, **MPTHP** exhibits E_{HOMO} values of (−4.33 eV) and E_{HOMO} (−2.60 eV), respectively.

As shown in Fig. 6, the inhibitor molecule's HOMO level was clearly placed on the *p*-tolyldiazenyl, pyrrol, and phenyl moieties, indicating that the nitrogen and oxygen atoms on the steel surface are the favorite positions for electrophilic attack. These explanations suggest that inhibitor molecules have the capacity to adhere to steel surface, growing the proficiency of inhibition in accordance with experimental evidence. Similar to this, the energy gap (ΔE) is a crucial sign of a molecule's capacity to suppress corrosion [57]. As shown in Table 5, **MPTHP** has a low E value (1.73 eV), which supports a higher propensity for being adsorbed on tested steel. Furthermore, the low electronegativity values (χ) similarly, suggest a possibility for increased responsiveness of the inhibitor particles to give electrons to the examined surface [58].

Additionally, the softness (σ) and hardness (η) of the compound may be used to figure out how reactive and stable it is. Soft particles, e.g., have higher defensive capabilities than hard particles because of the advantage of effectively delivering electrons to the tested surface by the adsorption progression, and are therefore presumed to be active corrosion inhibitors [59]. According to Table 5, **MPTHP** exhibits lower and higher values, which clearly denotes a greater inhibitor capacity for supplying electrons to the steel exterior as well as a large inhibition efficiency.

The larger the ΔN value, the further capable the tested inhibitor is of doing this [60]. The probability of the tested inhibitor to donate electrons to the steel surface is measured by the ΔN values. A back-donation from the inhibitor examined the electron as it went to a target molecule, will be 0 when $\eta > 0$ as well, and this is actively favored [61]. According to Table 5, the **MPTHP's** calculated $\Delta E_{back\text{-}donation}$ value is negative (−0.22), representing that back-donation is preferable for the **MPTHP** to form a long-lasting assembly with the steel surface [61].

Another important sign that helps with the analytical process of corrosion prevention is the dipole moment [62,63]. The improved molecule adsorption on the tested surface is a consequence of the rise in dipole moment, which also rises the deformation energy. Consequently, an increase in dipole moment values in an enhancement in corrosion inhibition [64,65].

Additionally, there is a connection between the inhibitor molecules' propensity for shielding the outside of steel in corrosive conditions and their molecular surface area. The efficacy of inhibition grows linearly with increasing inhibitor surface area, as shown by this equation. This is because there is more surface area amid the inhibitor molecues and the surface under test. In the analytical assessment of corrosion inhibition, the dipole moment serves as a significant signal, The electron-donating properties of the electron-

Table 5
MPTHP inhibitory efficiency was compared quantitatively to that of other azo dyes recently examined.

Inhibitor	Method	Corrosive Medium	Inhibitor, Conc	IE%	Ref
2,6-di-tert-butyl-4-(4-iodophenylazo)phenol. 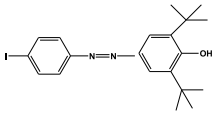	PP EIS	1 M HCl	1×10^{-4} M	71.65 89.40	[49]
(E)-2-((2,5-dichlorophenyl)diazenyl)naphthalen-1-ol 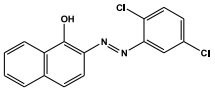	PP	0.5 M HCl	0.075 g	72.20	[50]
Mordant Green 17 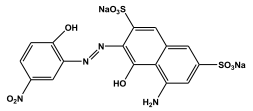	PP	1.0 M HCl	1×10^{-3} M	69.64	[51]
Mordant Orange 37 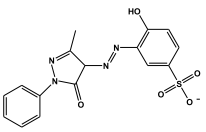	PP	1.0 M HCl	1×10^{-3} M	60.25	[51]
Woodstain Scarlet 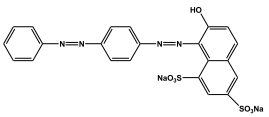	PP	1.0 M HCl	1×10^{-3} M	76.15	[51]
(L) 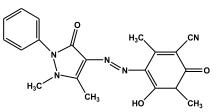	PP EIS	1.0 M HCl	25 mg/L	78.82 77.54	[52]
-(4-phenoxyphenylazo)-1-naphthol (AZN-2) 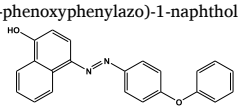	PP EIS	3.5 % sodium chloride solution	1×10^{-4} M	89.7 90.1	[53]
4-(4-pyridylazo)-1-naphthol (AZN-3) 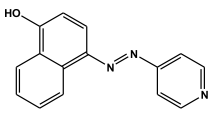	PP EIS	3.5 % sodium chloride solution	1×10^{-4} M	85.2 88.3	[53]
4-(2- pyridylazo)-1-naphthol (AZN-4) 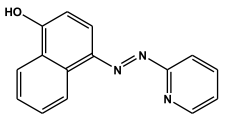	PP EIS	3.5 % sodium chloride solution	1×10^{-4} M	79.3 87.9	[53]
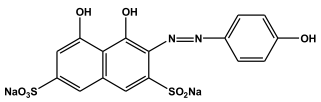	PP	0.5M sulfuric acid	2×10^{-2} M	73.1	[54]
Azo dye 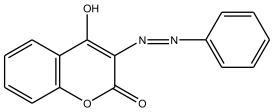	PP EIS	1.0 M HCl	1×10^{-3} M	89 90	[55]
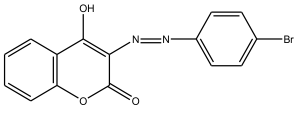	PP EIS	1.0 M HCl	1×10^{-3} M	83 89	[55]

(*continued on next page*)

Table 5 (*continued*)

Inhibitor	Method	Corrosive Medium	Inhibitor, Conc	IE%	Ref
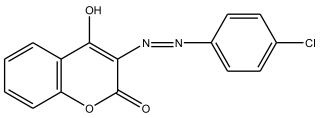	PP EIS	1.0 M HCl	1×10^{-3} M	86 89	[55]

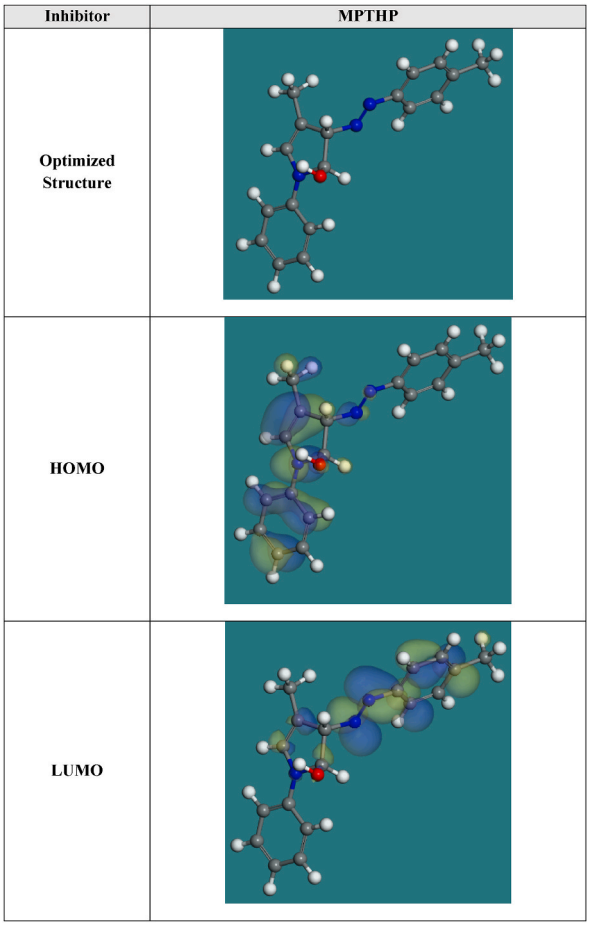

Fig. 6. The HOMO and LUMO molecular structures of the MPTHP derivative that were optimized using the DMol^3 module.

rich groups appear to be the source of the charge redistributions between the inhibitor molecules and iron atoms of steel [62–64]. The increased dipole moment, which simultaneously raises the deformation energy, leads to better compound adsorption on the tested metal. Therefore, an improvement in corrosion prevention consequences from a growth in dipole moment values [65,66].

Additionally, a correlation exists between a molecule's molecular surface area and an inhibitor molecule's propensity for maintaining the steel exterior in corrosive mediums. Because the interaction range among the inhibitor particles and the tested surface widens, the efficiency of the inhibition improves as the surface area grows.

Additionally, molecular electrostatic potential mapping (MEP) might investigate the **MPTHP** molecule's more active locations and could be quantified by via the Dmol^3 module. A 3D visual descriptor called MEP mapping is suggested for classifying the overall electrostatic effect according to a constituent of the general charge release [63]. In the MEP maps displayed in Fig. 7, the greatest electron density zone is indicated by the red colours, and the MEP is consistently negative (because of a nucleophilic reaction). On the other hand, the blue colours indicate the uppermost positive zone (electrophilic reaction) [66]. The *p*-tolyldiazenyl and phenyl moieties of the investigated component often have wider negative zones than the 1H-pyrrol-2-ol moiety, which has a lower electron density, consistent with an ocular study of Fig. 7. Instead, MEP in **MPTHP** inhibitor showed the most positive sites over hydrogen atoms. The investigated inhibitor's red areas, which have a high electron density, may be the best places for interactions with steel to provide a protective barrier that is certainly adsorbed.

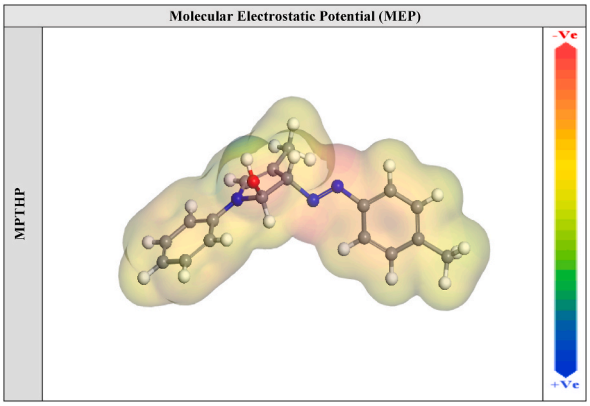

Fig. 7. Using DMol^3 module, graphical presentation of the MEP of **MPTHP** compound.

3.4. MC simulations

The objective of the Monte Carlo (MC) simulations was twofold: first, to identify the relations among the inhibitor particles and the tested steel exterior and second, to provide a visual representation of the adsorption process. Fig. 8 illustrates the most optimal configurations for the adsorption of MPTHP particles on steel exterior, as determined by the adsorption locator module. These configurations appear to be well-established and exhibit a relatively smooth character, suggesting an efficient adsorption process and maximum exposure of the inhibitor particles to the surface. This visual representation helps in understanding the adsorption mechanism and the favorable orientations of MPTHP on the examined metal [67]. Furthermore, Table 6 presents the outcomes of adsorption energy calculations derived from Monte Carlo (MC) simulations. As per the table, **MPTHP** exhibits a remarkably low adsorption energy value of −4327.86 kcal mol-1, indicative of its robust affinity for the test surface. These results, which correspond to a strongly adsorbed coating, are consistent with the experimental observations and support the notion that MPTHP effectively prevents corrosion and safeguards the steel surface [68]. Furthermore, Table 7 demonstrations that the **MPTHP** adsorption energies values for the

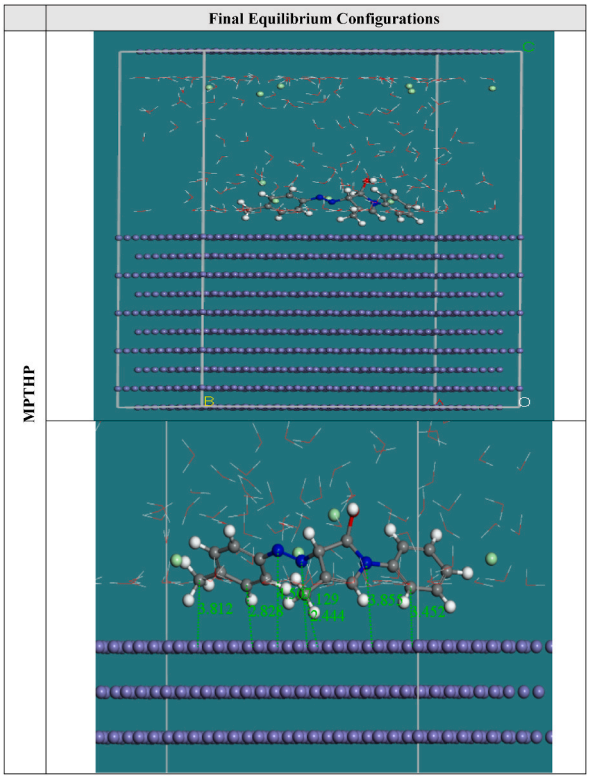

Fig. 8. The adsorption locator module's determination of the optimal configuration for MPTHP adsorption on Fe (1 1 0) substrate.

Table 6
The considered quantum chemical variables for the **MPTHP** derivatives.

Inhibitor	MPTHP
E_{HOMO}, eV	−4.33
E_{LUMO}, eV	−2.60
ΔE, eV	1.73
I	4.33
A	2.60
χ	3.47
η	0.86
σ	1.16
ΔN	2.05
$\Delta E_{back\text{-}donation}$, eV	−0.22
Dipole moment value, debye	2.68
Molecular surface area, $Å^2$	336.88

Table 7
Data and descriptors calculated by the Mont Carlo simulation for adsorption of tested **MPTHP** on Fe (1 1 0).

Structure	Adsorption energy	Rigid adsorption energy	Deformation energy	MPTHP: dE_{ads}/dN_i	Chloride: dE_{ads}/dNi	Water: dE_{ads}/dN_i
Fe (1 1 0)	−4327.86	−3357.89	−969.97	−292.84	−98.85	−18.13

unrelaxed pre-geometry optimization stage (−3357.89 $kcalmol^{-1}$) and relaxed post-geometry optimization step (−969.97 $kcalmol^{-1}$, respectively) indicate a better level of **MPTHP** proficiency.

The energy configuration of the metal-adsorbate system becomes evident through the dE_{ads}/dN_i values, particularly when an adsorbed inhibitor or water molecule is no longer present [69]. Table 6 displays the dE_{ads}/dN_i values for **MPTHP**, revealing a remarkable adsorption energy of (−292.84 kcal mol^{-1}). In contrast, the dE_{ads}/dN_i values for water are much lower at nearly (−18.13 kcal mol^{-1}). This significant disparity between **MPTHP** and water values indicates a stronger affinity of inhibitor molecules for adsorption compared to water molecules. This preference for inhibitor molecules suggests that they effectively displace water particles on the surface. Consequently, **MPTHP** derivatives unequivocally adhere to the steel surface, establishing a persistent protecting coating that poses a corrosion challenge for the steel specimen in corrosive solutions. This conclusion is corroborated by a combination of investigative and theoretical analyses.

3.5. Inhibition mechanism of MPTHP compound

Overall, the data from the various electrochemical techniques that were retrieved confirm that **MPTHP** compound did indeed prevent corrosion on N80 carbon steel exterior in 10 % HCl acidic solutions. The analyzed chemicals' adsorption on the investigated metal, which condensed the revealed surface area with the corrosive solutions, may be in authority for the proficiency of **MPTHP** inhibitors.

These explanations increase the adsorption of the tested **MPTHP** inhibitor since the designated **MPTHP** inhibitor has more than active sites for π-electron as aromatic benzene moieties and the incidence of certain heteroatoms as nitrogen. The 10 % HCl solution medium contains a protonated version of the **MPTHP** inhibitor [70]. The adsorption process may start with $-Cl^-$ anions being initially adsorbed on protonated steel surfaces to generate a negatively charged barrier because it is well recognized that N80 steel surfaces are (+ve) charged in hydrochloric acid solutions [71].

The concentration of anions on the outside of N80 would then regulate the adsorption of the protonated **MPTHP** component.

To process a coordinate bond with the unoccupied *d*-orbitals of N80 carbon steel (i.e., Fe) and create a protective chemisorbed wall, **MPTHP** compound can be adsorbed in a manner similar to Lewis' acid by forming donor-acceptor associations amid the free electron pairs of (N) heteroatoms and the π -electron of each double bond [72–74]. As shown in Fig. 9, the **MPTHP** compound of N80 carbon steel's chemisorption adsorption in acidified 10 % HCl solution was authorized using $\mathbf{\Delta G^{\circ}_{ads}}$ values that were computed and were greater than −40 kJ mol^{-1}. Last but not least, the existence of extra phenyl moiety active sites that are exposed to electrophilic attack with minimal HOMO energy, low $\mathbf{\Delta \boldsymbol{E}}$, and modest hardness is what accounts for the efficiency of **MPTHP's** inhibition [75].

According to DFT calculations, the tested inhibitor's nitrogen-containing hydrophilic groups serve as the primary sites for electrophilic attack. To increase their adsorption capacity, additional reactive sites and activities are provided by the inclusion of benzene rings and a C=C double bond. The inhibitor molecules' adsorption conformation on the steel surface indicates that the inhibitor's N-atoms and iron atoms are bonded. The MPTHP inhibitor was shown to adsorb on the steel surface in a parallel configuration by the molecular dynamics' simulation study, and the associated adsorption energies showed a good correlation with the inhibition efficiencies that were obtained experimentally [76].

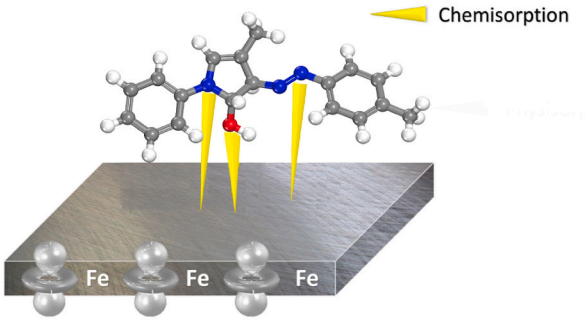

Fig. 9. Diagram of the mechanism of MPTHP adsorption on N80 steel surface.

4. Conclusions

The tested inhibitor, 4-methyl-1-phenyl-3-(*p*-tolyldiazenyl)-2,3-dihydro-1H-pyrrol-2-ol (**MPTHP**) is a reliable molecule for protecting N80 steel against corrosion in a 10 % HCl environment, functioning as a mixed-type inhibitor. Its effectiveness increases with higher concentrations, as shown by comprehensive electrochemical data as PP technique (90.6 %). Before introducing the **MPTHP** inhibitor, double-layer capacitances significantly decrease compared to a control 10 % HCl solution and inhibition efficiency reach to (91 %), likely due to the adsorption mechanism of **MPTHP** on the N80 steel surface, explained using the Langmuir adsorption isotherm. The negative sign of ΔG^{o}_{ads} indicates the spontaneity of the adsorption process. The consistency of inhibition efficiency values from various electrochemical techniques (PP and EIS) accepts with DFT calculations and MC simulations, correctness and integrity of the results and computational data.

CRediT authorship contribution statement

Reham H. Wahba: Data curation, Investigation, Methodology. **Adel Z. El-Sonbati:** Writing – original draft, Writing – review & editing. **Mostafa A. Diab:** Conceptualization, Investigation, Methodology. **Esam A. Gomaa:** Formal analysis, Supervision, Writing – original draft. **Marwa N. El-Nahass:** Investigation, Methodology, Writing – original draft. **Y.M. Abdallah:** Conceptualization, Data curation, Funding acquisition, Investigation, Methodology, Software, Supervision, Writing – original draft, Writing – review & editing.

Declaration of competing interest

The authors declare that they have no known competing financial interests or personal relationships that could have appeared to influence the work reported in this paper.

References

[1] Hany M. Abd El-Lateef, Kamal Shalabi, Anas M. Arab, Yasser M. Abdallah, Corrosion mitigation performance of N80 steel in 5% sulfamic acid medium by applying novel tetrahydro-1,2,4-triazines including triazene moieties: electrochemical and theoretical approaches, ACS Omega 7 (2022) 23380–23392, https://doi.org/10.1021/acsomega.2c01629.
[2] J. Carneiro, J. Tedim, Ferreira, Chitosan as a smart coating for corrosion protection of aluminum alloy 2024, Prog. Org. Coating 89 (2015) 348–356, https://doi.org/10.1016/j.porgcoat.2015.03.008.
[3] M. Finšgar, J. Jackson, Application of corrosion inhibitors for steels in acidic media for the oil and gas industry, Corrosion Sci. 86 (2014) 17–41, https://doi.org/10.1016/j.corsci.2014.04.044.
[4] E. Vazirinasab, R. Jafari, G. Momen, Evaluation of atmospheric-pressure plasma parameters to achieve superhydrophobic and self-cleaning HTV silicone rubber surfaces via a single-step, eco-friendly approach, Surf. Coat. Technol. 341 (2017) 40–56, https://doi.org/10.1016/j.surfcoat.2019.07.005.
[5] N. Chafai, S. Chafaa, K. Benbouguerra, Synthesis, characterization and the inhibition activity of a new α-aminophosphonic derivative on the corrosion of XC48 carbon steel in 0.5 M H_2SO_4: experimental and theoretical studies, J. Taiwan Inst. Chem. Eng. 70 (2017) 331–344, https://doi.org/10.1016/j.jtice.2016.10.026.
[6] M. Lebrini, F. Robert, H. Vezin, C. Roos, Electrochemical and quantum chemical studies of some indole derivatives as corrosion inhibitors for C38 steel in molar hydrochloric acid, Corrosion Sci. 52 (2010) 3367–3376, https://doi.org/10.1016/j.corsci.2010.06.009.
[7] S. Zhang, Z. Tao, W. Li, B. Hou, The effect of some triazole derivatives as inhibitors for the corrosion of mild steel in 1 M hydrochloric acid, Appl. Surf. Sci. 255 (2009) 6757–6763, https://doi.org/10.1016/j.apsusc.2008.09.089.
[8] L.M. Vračar, D.M. Dražić, Adsorption and corrosion inhibitive properties of some organic molecules on iron electrode in sulfuric acid, Corrosion Sci. 44 (2002) 1669–1680, https://doi.org/10.1016/S0010-938X(01)00166-4.
[9] M.J. Bahrami, S.M.A. Hosseini, P. Pilvar, Experimental and theoretical investigation of organic compounds as inhibitors for mild steel corrosion in sulfuric acid medium: corrs, Science 52 (2010) 2793–2803, https://doi.org/10.1016/j.corsci.2010.04.024.
[10] D. Wang, B. Xiang, Y. Liang, Corrosion control of copper in 3.5 wt.% NaCl solution by domperidone: experimental and theoretical study, Corrosion Sci. 85 (2014) 77–86, https://doi.org/10.1016/j.corsci.2014.04.002.
[11] M.K. Pavithra, T.V. Venkatesha, M.K. Punith Kumar, H.C. Tondan, Inhibition of mild steel corrosion by Rabeprazole sulfide: corrs, Science 60 (2012) 104–111, https://doi.org/10.1016/j.corsci.2012.04.003.
[12] N. Benzbiria, A. Thoume, S. Echihi, M.E. Belghiti, A. Elmakssoudi, A. Zarrouk, M. Azzi, M. Zertoubi, Coupling of experimental and theoretical studies to apprehend the action of benzodiazepine derivative as a corrosion inhibitor of carbon steel in 1M HCl, J. Mol. Struct. 1281 (2023) 135139, https://doi.org/10.1016/j.molstruc.2023.135139.
[13] Samir H. Shafek, Eman A. Ghiaty, Nasser M. El Basiony, Emad A. Badr, Samy M. Shaban, Preparation of zwitterionic ionic surfactants-based sulphonyl for steel protections: experimental and theoretical insights, Z. Phys. Chem. 237 (1–2) (2023) 1–33, https://doi.org/10.1515/zpch-2022-0135.

[14] A.A. Al-Sarawy, A.S. Fouda, W.A.S. El-Dein, Some thiazole derivatives as corrosion inhibitors for carbon steel in acidic medium, Desalination 229 (2008) 279–293, https://doi.org/10.1016/j.desal.2007.09.013.

[15] A. Chetouani, B. Hammouti, T. Benhadda, Daoudi, inhibitive action of bipyrazolic type organic compounds towards corrosion of pure iron in acidic media, Appl. Surf. Sci. 249 (8) (2005) 375–385, https://doi.org/10.1016/j.apsusc.2004.12.034.

[16] A.S. Fouda, A.H. El-azaly, R.S. Awad, A.M. Ahmed, New benzonitrile azo dyes as corrosion inhibitors for carbon steel in hydrochloric acid solutions, Int. J. Electrochem. Sci. 9 (2014) 1117–1131, https://doi.org/10.1016/S1452-3981(23)07782-9.

[17] M. Abdallah, M.M. Alfakeer, N.F. Hasan, A.M. Alharbi, E.M. Mabrouk, Polarographic performance of some azo derivatives derived from 2-amino-4-hydroxy pyridine and its inhibitory effect on C-steel corrosion in hydrochloric acid, Orient. J. Chem. 35 (2019) 98, https://doi.org/10.13005/ojc/350111.

[18] M. Abdallah, B.H. Asghar, I. Zaafarany, A.S. Fouda, The inhibition of carbon steel corrosion in hydrochloric acid solution using some phenolic compounds, Int. J. Electrochem. Sci. 7 (2012) 282–304, https://doi.org/10.1016/S1452-3981(23)13338-4.

[19] Mohammad Mouayad Ahmed, Mehdi Salih Shihab, Pyridinium bromide derivatives as corrosion inhibitors for mild steel in 1M H_2SO_4, Egypt. J. Chem. 66 (2) (2023) 63–72, https://doi.org/10.21608/ejchem.2022.126742.5625.

[20] E.Q. Jasim, Investigation of Salvadora persica roots extract as corrosion inhibitor for mild steel in 1 M HCl and in cooling water, Chem. Mater. Res. 7 (2015) 147–159.

[21] Y. Abboud, A. Abourriche, T. Saffaj, M. Berrada, M. Charrouf, A. Bennamara, H. Hannache, A novel azo dye, 8-quinolinol-5-azoantipyrine as corrosion inhibitor for mild steel in acidic media, Desalination 237 (2009) 175–189, https://doi.org/10.1016/j.desal.2007.12.031.

[22] A. Ismail, A review of green corrosion inhibitor for mild steel in seawater, ARPN J. Eng. Appl. Sci. 11 (2016) 8710–8714.

[23] E.M. Mabrouk, H. Shokry, K.M.A.B.U. Alnaja, Inhibition of aluminum corrosion in acid solution by mono- and bis-azo naphthylamine dyes, Chemistry of metals and alloys, Part 1 (4) (2011) 98–106, https://doi.org/10.30970/cma4.0168.

[24] I.A. Mohammed, A. Mohammed, Synthesis of new azo compounds based on n-(4- hydroxypheneyl)maleimide and n-(4- methylpheneyl)maleimide, Molecules 15 (2010) 7498–7508, https://doi.org/10.3390/molecules15107498.

[25] F. Touhami, A. Aouniti, Y. Abed, B. Hammouti, S. Kertit, A. Ramdani, K. Elkacemi, Corrosion inhibition of armco iron in 1 M HCl media by new bipyrazolic derivatives, Corrosion Sci. 42 (2000) 929–940, https://doi.org/10.1016/S0010-938X(99)00123-7.

[26] A.S. Fouda, M. Gaber, M. Fakeeh, Azo Compounds as Green Corrosion Inhibitor for Carbon Steel in Hydrochloric Acid Solution : Corrosion Inhibition and Thermodynamic Parameters, vol. 12, 2017, pp. 8745–8760, https://doi.org/10.20964/2017.09.33.

[27] R.G. Parr, R.A. Donnelly, M. Levy, W. Palke, E, Electronegativity: the density functional viewpoint, J. Chem. Phys. 68 (1978) 3801–3807, https://doi.org/10.1063/1.436185.

[28] M. Stern, Closure to "discussion of 'electrochemical polarization, 1. A theoretical analysis of the shape of polarization curves', in: M. Stern, A.L. Geary (Eds.), J. Electrochem. Soc. 104 (1957) 751–758, https://doi.org/10.1149/1.2428473, pp. 56–63, vol. 104.

[29] M.A. Deyab, G. Mele, Polyaniline/Zn-phthalocyanines nanocomposite for protecting zinc electrode in Zn-air battery, J. Power Sources 443 (2019) 227264, https://doi.org/10.1016/j.jpowsour.2019.227264.

[30] H.M. Abd El-Lateef, K. Shalabi, A.A. Abdelhamid, One-pot synthesis of novel triphenyl hexyl imidazole derivatives catalyzed by ionic liquid for acid corrosion inhibition of C1018 steel: experimental and computational perspectives, J. Mol. Liq. 334 (2021) 116081, https://doi.org/10.1016/j.molliq.2021.116081.

[31] D.K. Verma, R. Aslam, J. Aslam, M.A. Quraishi, E.E. Ebenso, C. Verma, Computational modeling: theoretical predictive tools for designing of potential organic corrosion inhibitors, J. Mol. Struct. 1236 (2021) 130294, https://doi.org/10.1016/j.molstruc.2021.130294.

[32] Y.M. Abdallah, Hesham Elzanaty, Electrochemical studies on the inhibition behavior of composite Udimet 700 – alumina in 1 M hydrochloric acid by some new organic derivatives, Mater. Chem. Phys. 238 (2019) 121925, https://doi.org/10.1016/j.matchemphys.2019.121925.

[33] A.Y. Yassin, A.M. Abdelghany, M.M. Shaban, Y.M. Abdallah, Synthesis, characterization and electrochemical behavior for API 5L X70 carbon steel in 5% sulfamic acid medium using PVVH/PEMA blend filled with gold nanoparticles, Journal of Colloids and Surfaces A: Physicochemical and Engineering Aspects 635 (2022) 128115, https://doi.org/10.1016/j.colsurfa.2021.128115.

[34] F. Bentiss, M. Lebrini, H. Vezin, F. Chai, M. Traisnel, M. Lagrene, Enhanced corrosion resistance of carbon steel in normal sulfuric acid medium by some macrocyclic polyether compounds containing a 1,3,4-thiadiazole moiety: AC impedance and computational studies, Corrosion Sci. 51 (9) (2009) 2165–2173, https://doi.org/10.1016/j.corsci.2009.05.049.

[35] Maryam Chafiq, Abdelkarim Chaouik, Mustafa R. Al-Hadeethi, Rachid Salgh, Ismat H. Ali, Shaaban K. Mohamed, Il-Min Chung, A joint experimental and theoretical investigation of the corrosion inhibition behavior and mechanism of hydrazone derivatives for mild steel in HCl solution, Colloids Surf. A Physicochem. Eng. Asp. 610 (2021) 125744, https://doi.org/10.1016/j.colsurfa.2020.125744.

[36] S.A. Umoren, U.F. Ekanem, Inhibition of mild steel corrosion in H_2SO_4 using exudate gum from pachylobus edulis and synergistic potassium halide additives, Chem. Eng. Commun. 197 (2010) 1339–1356, https://doi.org/10.1080/00986441003626086.

[37] M.G. Hosseini, S.F.L. Mertens, M. Ghorbani, M.R. Arshadi, Asymmetrical Schiff bases as inhibitors of mild steel corrosion in sulphuric acid media, J. Mater. Chem. Phys. 78 (3) (2003) 800–808, https://doi.org/10.1016/S0254-0584(02)00390-5.

[38] B.B. Damaskin, O.A. Petrii, V.V. Batrakov, Adsorption of Organic Compounds on Electrodes, Plenum Press, New York, 1971.

[39] J. Lipkowski, P.N. Ross (Eds.), Adsorption of Molecules at Metal Electrodes, VCH, New York, 1992, 0895737868, 9780895737861.

[40] E. Khamis, F. Bellucci, R.M. Latanision, E.S.H. El-Ashry, Acid corrosion inhibition of nickel by 2-(Triphenosphoranylidene) succinic anhydride, Corrosion 47 (9) (1991) 677–686, https://doi.org/10.5006/1.3585307.

[41] O.E. Barcia, O.R. Mattos, N. Pebere, B. Tribollet, J. Electrochem. Soc. 140 (1993) 2825, https://doi.org/10.1149/1.2220917.

[42] K. Juttner, Electrochemical impedance spectroscopy (EIS) of corrosion processes on inhomogeneous surfaces, Electrochim. Acta 35 (1990) 1501–1508, https://doi.org/10.1016/0013-4686(90)80004-8.

[43] D.A. Lopez, S.N. Simison, S.R. de Sanchez, Inhibitors performance in CO_2 corrosion EIS studies on the interaction between their molecular structure and steel microstructure, Corrosion Sci. 47 (2005) 735–755, https://doi.org/10.1016/0013-4686(90)80004-8.

[44] J.R. Macdonald, Impedance Spectroscopy, John Wiley & Sons, Inc, New York, 1987, pp. 289–305.

[45] F. Rosalbino, G. Scavino, G. Mortarino, E. Angelini, G. Lunazzi, EIS study on the corrosion performance of a Cr (III)-based conversion coating on zinc galvanized steel for the automotive industry, J. Solid State Electrochem. 15 (2011) 703–709, https://doi.org/10.1007/s10008-010-1140-7.

[46] Mengyue Zhu, Zhong yi He, Lei Guo, Renhui Zhang, Valentine Chikaodili Anadebe, Bassey Obot Ime, Xingwen Zheng, Corrosion inhibition of eco-friendly nitrogen-doped carbon dots for carbon steel in acidic media: performance and mechanism investigation, J. Mol. Liq. 342 (2021) 117583, https://doi.org/10.1016/j.molliq.2021.117583.

[47] Mengqin Zhang, Lei Guo, Mengyue Zhu, Kai Wang, Renhui Zhang, Zhongyi He, Yuanhua Lin, Senlin Leng, Valentine Chikaodili Anadebe, Xingwen Zheng, Akebia trifoliate koiaz peels extract as environmentally benign corrosion inhibitor for mild steel in HCl solutions: integrated experimental and theoretical investigations, J. Ind. Eng. Chem. 101 (2021) 227236, https://doi.org/10.1016/j.jiec.2021.06.009.

[48] Abdallah Metwally, Nizar El Guesmi, Arej S. Al-Gorair, Refat El-Sayed, Meshabi Aseel, Sobhi Mohamed, Enhancing the anticorrosion performance of mild steel in sulfuric acid using synthetic non-ionic surfactants: practical and theoretical studies, Green Chem. Lett. Rev. 14 (2) (2021) 382394, https://doi.org/10.1080/17518253.2021.1921858.

[49] Mostafa M. Khalefa, Hazem F. Khalil, S.T. Keera, Ashraf M. Ashmawy, Preparation and evaluation of Azo phenol as corrosion inhibitor for carbon steel in acid solution. Egypt, J. Chem. 65 (5) (2022) 791–802, https://doi.org/10.21608/EJCHEM.2022.142387.6224.

[50] Justinah Amoko, Olawale Akinyele, Dare Olayanju, Augustus Oluwafemi, Christopher Aboluwoye, Synthesis, corrosion inhibition and theoretical studies of (E)-2-((2,5-Dichlorophenyl) diazenyl) naphthalen-1-ol as corrosion inhibitor of mild steel in 0.5 M hydrochloric acid, Chem. Mater. Res. 10 (6s) (2018).

[51] A.M. Nagiub, M.H. Mahross, H.F.Y. Khalil, B.N.A. Mahran, M.M. Yehia, M.M.B. El-Sabbah, Azo dye compounds as corrosion inhibitors for dissolution of mild steel in hydrochloric acid solution, Port. Electrochim. Acta 31 (2) (2013) 119–139, https://doi.org/10.4152/pea.201302119.

[52] B.G. Devika, B.H. Doreswamy, H.C. Tandon, Corrosion behaviour of metal complexes of antipyrine based azo dye ligand for soft-cast steel in 1 M hydrochloric acid, J. King Saud Univ. Sci. 32 (2020) 881–890, https://doi.org/10.1016/j.jksus.2019.04.007.

[53] K. Shalabi, M.H. Abd El-Lateef, M.M. Hammouda, A.A. Abdelhamid, Green synthesizing and corrosion inhibition characteristics of azo compounds on carbon steel under sweet conditions: experimental and theoretical approaches, ACS Omega 9 (2024) 18932–18945, https://doi.org/10.1021/acsomega.3c09072.
[54] E.M. Mabrouk, S. Eid, M.M. Attia, Corrosion inhibition of carbon steel in acidic medium using azo chromotropic acid dye compound, Journal of Basic and Environmental Sciences 4 (2017) 351–355, https://doi.org/10.21608/jbes.2017.369737.
[55] H.M. Yusoff, N.M. Azmi, H.M.d Hussin, H. Osman, B.P. Raja, A.A. Rahim, K. Awang, An electrochemical evaluation of synthesized coumarin-azo dyes as potential corrosion inhibitors for mild steel in 1 M HCl medium, Int. J. Electrochem. Sci. 15 (2020) 11742–11756, https://doi.org/10.20964/2020.12.43.
[56] M. Boulhaoua, M. El Hafi, S. Zehra, L. Eddaif, A.A. Alrashdi, S. Lahmidi, L. Guo, J.T. Mague, H. Lgaz, Synthesis, structural analysis and corrosion inhibition application of a new indazole derivative on mild steel surface in acidic media complemented with DFT and MD studies, Colloids Surfaces A: physicochem, Eng. Asp. 617 (2021) 126373.
[57] Hany M. Abd El-Lateef, K. Shalabi, H. Tantawy Ahmed, Corrosion inhibition and adsorption features of novel bioactive cationic surfactants bearing benzenesulphonamide on C1018-steel under sweet conditions: combined modeling and experimental approaches, J. Mol. Liq. 320 (2020) 114564–114584, https://doi.org/10.1016/j.molliq.2020.114564.
[58] N. Palaniappan, I.S. Cole, A.E. Kuznetsov, Experimental and computational studies of graphene oxide covalently functionalized by octylamine: electrochemical stability, hydrogen evolution, and corrosion inhibition of the AZ13 Mg alloy in 3.5% NaCl, RSC Adv. 10 (2020) 11426–11434, https://doi.org/10.1039/C9RA10702A.
[59] I.B. Obot, D.D. Macdonald, Z.M. Gasem, Density functional theory (DFT) as a powerful tool for designing new organic corrosion inhibitors. Part 1: an overview, Corrosion Sci. 99 (2015) 1–30, https://doi.org/10.1016/j.corsci.2015.01.037.
[60] I. Lukovits, E. Kálmán, F. Zucchi, Corrosion inhibitors-correlation between electronic structure and efficiency, Corrosion 57 (2001) 3–8, https://doi.org/10.5006/1.3290328.
[61] A. Upadhyay, A. Kumar, G. Mahakur, S. Dash, P. Kumar, Verification of corrosion inhibition of Mild steel by some 4-Aminoantipyrine-based Schiff bases –Impact of adsorbate substituent and cross-conjugation, J. Mol. Liq. 333 (2021) 115960, https://doi.org/10.1016/j.molliq.2021.115960.
[62] Hany M. Abd El-Lateef, K. Shalabi, H. Tantawy Ahmed, Corrosion inhibition of carbon steel in hydrochloric acid solution using newly synthesized urea-based cationic fluorosurfactants: experimental and computational investigations, New J. Chem. 44 (2020) 17791–17814, https://doi.org/10.1039/D0NJ04004E.
[63] A.K. Oyebamiji, B.B. Adeleke, Quantum chemical studies on inhibition activities of 2,3 dihydroxypropyl-sulfanyl derivative on carbon steel in acidic media, Int. J. Corros. Scale Inhib. 7 (2018) 498–508, https://doi.org/10.17675/2305-6894-2018-7-4-2.
[64] Lei Guo, Chengwei Qi, Xingwen Zheng, Renhui Zhang, Xun Shena, Savaş Kaya, Toward understanding the adsorption mechanism of large size organic corrosion inhibitors on an Fe(110) surface using the DFTB method, RSC Adv. 7 (2017) 29042–29050, https://doi.org/10.1039/c7ra04120a.
[65] L.H. Madkour, S. Kaya, I.B. Obot, Computational, Monte Carlo simulation and experimental studies of some arylazotriazoles (AATR) and their copper complexes in corrosion inhibition process, J. Mol. Liq. 260 (2018) 351–374, https://doi.org/10.1016/j.molliq.2018.01.055.
[66] G. Gece, S. Bilgiç, Quantum chemical study of some cyclic nitrogen compounds as corrosion inhibitors of steel in NaCl media, Corrosion Sci. 51 (2009) 1876–1878, https://doi.org/10.1016/j.corsci.2009.04.003.
[67] K. Shalabi, A.M. Helmy, A.H. El-Askalany, M.M. Shahba, New pyridiniumbromidemono-cationic surfactant as corrosion inhibitor for carbon steel during chemical cleaning: experimental and theoretical studies, J. Mol. Liq. 293 (2019) 111480–111494, https://doi.org/10.1016/j.molliq.2019.111480.
[68] H. El Aadad, M. Galai, M. Ouakki, A. Elgendy, M.E. Touhami, A. Chahine, Improvement of the corrosion resistance of mild steel in sulfuric acid by new organic-inorganic hybrids of Benzimidazole-Pyrophosphate: facile synthesis, characterization, experimental and theoretical calculations (DFT and MC), Surface. Interfac. 24 (2021) 101084, https://doi.org/10.1016/j.surfin.2021.101084.
[69] A. Dehghani, A.H. Mostafatabar, G. Bahlakeh, B. Ramezanzadeh, A detailed study on the synergistic corrosion inhibition impact of the Quercetin molecules and trivalent europium salt on mild steel; electrochemical/surface studies, DFT modeling, and MC/MD computer simulation, J. Mol. Liq. 316 (2020) 113914–113930, https://doi.org/10.1016/j.molliq.2020.113914.
[70] M. Abdallah, H.E. Megahed, Cyclic voltammograms of iron and C-steels in oxalic acid solutions and investigation of the effect of phenyl phthalimide as corrosion inhibitors, Monatsh. Chem. 126 (1995) 519–527. https://link.springer.com/article/10.1007/BF00807424.
[71] R. Solmaz, G. Kardas, B. Yazc, M. Erbil, Adsorption and corrosion inhibitive properties of 2-amino-5-mercapto-1,3,4-thiadiazole on mild steel in hydrochloric acid media, Colloids Surf. A Physicochem. Eng. Aspects 312 (2008) 7–17, https://doi.org/10.1016/j.colsurfa.2007.06.035.
[72] E. Blomgren, J.O.M. Bockris, The adsorption of aromatic amines at the interface: mercury-aqueous acid solution, J. Phys. Chem. 63 (1959) 1475–1484, https://doi.org/10.1021/j150579a037.
[73] I. Ahamad, M.A. Quraishi, Mebendazole: new and efficient corrosion inhibitor for mild steel in acid medium, Corrosion Sci. 52 (2010) 651–656, https://doi.org/10.1016/j.corsci.2009.10.012.
[74] F. Bentiss, M. Lebrini, M. Lagrenee, Thermodynamic characterization of metal dissolution and inhibitor adsorption processes in mild steel/2,5-bis(nthienyl)-1,3,4-thiadiazoles/hydrochloric acid system, Corrosion Sci. 47 (2005) 2915–2931, https://doi.org/10.1016/j.corsci.2005.05.034.
[75] D. Kumar, N. Jain, V. Jain, B. Rai, Amino acids as copper corrosion inhibitors: a density functional theory approach, Appl. Surf. Sci. 514 (2020) 145905, https://doi.org/10.1016/j.apsusc.2020.145905.
[76] Fangyuan Wan, Shihao Zhang, Baimei Tan, Yunhui Shi, Xiaolong Wang, Haoyu Du, Renhao Liu, Xinyu Han, Three anionic surfactants for corrosion inhibition in cobalt CMP: research on validity and mechanism, Surface. Interfac. 47 (2024) 104202, https://doi.org/10.1016/j.surfin.2024.104202.